Catalysis Today 139 (2009) 299–311

Contents lists available at ScienceDirect

Catalysis Today

journal homepage: www.elsevier.com/locate/cattod

Hydrogen generation and purification in a composite Pd hollow fiber membrane reactor: Experiments and modeling

Sameer H. Israni, Balamurali Krishna R. Nair, Michael P. Harold *

Department of Chemical and Biomolecular Engineering, University of Houston, S222 Engineering Building 1, Houston, TX 77204-4004, United States

ARTICLE INFO

Article history:
Available online 15 May 2008

Keywords:
Hydrogen
Ammonia
Palladium
Membrane reactor
Inorganic membrane

ABSTRACT

"Pd nanopore" composite membranes are a novel class of H_2 permselective membranes in which a thin layer of Pd is grown within the pores of a supported nanoporous layer. In this work, Pd nanopore membranes and conventional Pd top-layer membranes were used in the generation of high-purity H_2 from the catalytic decomposition of anhydrous NH_3. An effective 4 μm thick Pd nanopore membrane and 13 μm thick Pd top-layer membrane were synthesized on 2 mm O.D. α-Al_2O_3 hollow fibers. The permeation features of the membranes were determined and the membranes were then employed in a single fiber packed-bed membrane reactor in which Ni-catalyzed NH_3 decomposition served as the test reaction, with conditions spanning a range of conditions (500–600 °C; 3–5 bar total retentate pressure; 60–1200 scc/h g cat space velocity). The NH_3 conversions in both the PBMRs were approximately 10% higher than in a packed-bed reactor (PBR) under similar conditions. The increase in conversion with the PBMR was attributed to the removal of H_2, which has an inhibitory effect on the forward kinetics of the reaction as per the Temkin-Pyzhev type rate mechanism. Reactor productivities in the range of 2 mol/s m^3 (at 85% H_2 utilization) to 7 mol/s m^3 (at 50% H_2 utilization) were obtained. The permeate stream purity exceeded 99.2% H_2. A two-dimensional pseudo-homogeneous model was successfully used to simulate the experimental results and to interpret the findings. Permeation and kinetic parameters were estimated in permeation and PBR experiments, respectively. Without any data fitting the PBMR model predictions demonstrated very good agreement with experimental trends. Together with an analysis of the characteristic times, the model determined that transverse transport of hydrogen in the catalyst bed limited PBMR performance. The model was used to determine the rate limiting step and to suggest ways in which the reactor productivities could be further improved.

1. Introduction

The discovery that hydrogen permeates through palladium metal was made in 1863 [1]. Since then there has been extensive research in the area of using palladium to separate and purify hydrogen. During the last 10–15 years several small scale technologies based on Pd membranes have been developed to produce high-purity hydrogen at remote sites and for industrial, laboratory or military uses [2]. These applications mostly used self-supported Pd and Pd-alloy sheets of thickness of 50–100 μm.

Due to the increased concerns of greenhouse gas emissions, air pollution and future energy supply, the generation and purification of hydrogen is emerging as an important technology for portable power applications of proton exchange membrane (PEM) fuel cells. Membrane reactors offer a clear advantage over conventional schemes in terms of reactor productivity due to the consolidation of reaction, separation, and purification in a single unit [3,4]. The specific class of Pd-based membrane reactors affords potential for high-purity hydrogen production. There has been renewed interest in these multi-functional reactors in applications requiring compact, on-demand delivery of high-purity hydrogen. The main hurdles to commercialization include the high cost and unproven durability of Pd and Pd-based films for extended use, especially with swings in temperature and during exposure to certain species [1]. Membrane permeator performance targets have been defined by US Department of Energy (DOE) [5], which include an H_2 flux exceeding 1 mol/m^2/s (at 400 °C and a H_2 partial pressure differential of 20 psi) and a H_2 permeate purity of at least 99.99%. In a reactor application, volume productivity (or space–time yield) exceeding 50 mol/m^3 s is desirable [6] and a permeate hydrogen purity that achieves 99.99%, corresponding to an impurity level less than 1000 ppm.

* Corresponding author. Tel.: +1 713 743 4307; fax: +1 713 743 4323.
E-mail address: mharold@uh.edu (M.P. Harold).

0920-5861/$ – see front matter © 2008 Elsevier B.V. All rights reserved.
doi:10.1016/j.cattod.2008.02.020

Nomenclature

C_i	gas phase concentration of ith component (mol/m^3)
CPH	degree of H_2 concentration polarization
d	diameter of catalyst particles (m)
$D_{i,er}$	effective radial dispersion coefficient for the ith component (m^2/s)
D_r	inside diameter of packed bed (m)
Da	Damkohler number
E_H	permeance activation energy (J/mol)
F_i	molar flow rate of ith component (mol/s)
J_i	flux of ith species across membrane (mol/m^2 s)
k	rate parameter for NH_3 decomposition (mol/m^3/s)
K	rate parameter for NH_3 decomposition (bar$^{0.5}$)
L	length of the reactor (m)
$N_{Re} = d v \rho/\varepsilon\mu$	Reynolds number based on catalyst particle size
P_i	partial pressure of ith component (bar)
P_0	total retentate pressure (bar)
$Pe_{i,r}{}' = v_o R^2/D_{i,er}L$	modified transverse Peclet number for ith component
Pe_t	transverse Peclet number
q	membrane permeance (mol/s m^2 bar$^{0.5}$)
q_o	permeance pre-exponential factor
r	radial distance (m)
r_m	outer radius of Pd fiber (m)
R	inner radius of packed bed (m)
$\Re$	Universal gas constant
S_m	membrane surface area (m^2)
Sc	Schmidt number
T	temperature (K)
v	superficial gas velocity (m/s)
$v' = v/v_o$	dimensionless gas velocity
v_o	inlet superficial gas velocity (m/s)
V_r	reactor volume (m^3)
x_i	mole fraction of ith component
Y_{H_2}	hydrogen utilization in the membrane reactor
z	axial distance (m)
$Z = z/L$	dimensionless axial distance

Greek letters

ϑ_i	stoichiometric coefficient for the ith component
Λ	ratio of characteristic time of radial transport to characteristic permeation time
Π	hydrogen productivity of the reactor (mol/s/m^3)
α	ideal H_2/N_2 separation factor
ε	catalyst bed porosity
$\phi = QRP_0{}^{0.5}/\delta D_{i,er}C_0$	non-dimensional parameter (equivalent to ratio of radial diffusion characteristic time to permeation characteristic time)
γ	rate of reaction (mol/s/m^3)
$\gamma' = \gamma/\gamma(C_i^0)$	non-dimensional reaction rate
μ	gas viscosity (N s/m^2)
ρ	gas density (kg/m^3)
ρ_c	catalyst bed density (kg/m^3)
τ	catalyst bed tortuosity
τ_d	characteristic radial transport time (s)
τ_f	characteristic flow time (s)
τ_p	characteristic permeation time (s)
τ_r	characteristic reaction time (s)
$\xi = r/R$	dimensionless radial distance

Subscript

H_2	hydrogen
N_2	nitrogen
NH_3	ammonia

Superscript

perm	permeate side value of the parameter
ret	retentate side value of the parameter
0	initial value of the parameter

One way to increase flux and reduce cost is to reduce the thickness of the Pd layer. It has been suggested that thickness of pure Pd film should be <14 μm in order to achieve a target cost of \$150 ft^{-2} [7]. However, in general, as the Pd-membrane thickness is decreased the permselectivity decreases and the durability deteriorate. The minimum thickness required for a defect-free membrane is determined in part by the pore size of the substrate. Yildirim et al. [8] found that for defect-free membrane a minimum Pd thickness of 4 μm is required on a Vycor^{TM} glass substrate of 4 nm pore size. Defect-free membranes with thicknesses less than 2 μm can be synthesized using CVD or other sputtering methods. Composite Pd membranes are prepared by coating a layer of Pd directly onto the porous substrate using techniques like electroless plating (ELP), chemical vapor deposition (CVD), or sputtering. ELP is the more practical method in commercial practice compared to CVD and other techniques [9,10]. ELP can be carried out at low to moderate temperatures (25–80 °C) and a variety of substrates with the ability for in situ film thickness control. Yeung and Varma have demonstrated improved membrane characteristics and durability by employing an osmotic-driven ELP technique [11]. The investigators showed that the combination of smaller grain size and penetration into the underlying support led to membranes with fewer defects and good durability [12].

Recently our group has developed the so-called "Pd nanopore" and "Pd encapsulated" hollow fiber membranes that involve the combination of sol–gel slip casting and film coating with ELP [13]. These membranes have been shown to have good flux and permselectivity and appear to be more resilient than their top-layer counterparts. In the nanopore synthesis technique the addition of Pd nucleation sites onto a γ-Al_2O_3 is followed by another coating of γ-Al_2O_3. During the subsequent ELP step the Pd deposition takes place inside the pores of the second γ-Al_2O_3 layer. This sequence of steps ensures that the pores are completely filled, irrespective of the pore size of the substrate. Depending on the duration of the ELP step, Pd film growth may proceed beyond the pore mouths of the top alumina layer. The very good permeation features of the Pd nanopore and encapsulated membranes together with the potential for higher surface to volume ratios motivated us to examine their use in a high temperature reaction and separation.

In the current study we apply the Pd nanopore hollow fiber membrane in a packed-bed catalytic reactor. The model reaction that is considered is the catalytic decomposition of ammonia on a supported nickel catalyst. Ammonia decomposition is a mildly endothermic reversible reaction:

$$NH_3 \leftrightarrow 0.5N_2 + 1.5H_2, \quad \Delta H = +46.2\,\text{kJ/mol} \tag{1}$$

To this end, equilibrium conversion limitations are not important at sufficiently high temperatures (>450 °C). Compared to other hydrogen-carrying substances or fuels, ammonia has a rather high hydrogen-carrying capacity (~18 wt%), and liquid ammonia has a vapor pressure of about 8 bar at 25 °C, making it easy to store. NH_3 decomposition is an attractive option for producing H_2 for fuel cell and portable applications [14]. On the other hand, ammonia is toxic in high concentrations and noxious at lower concentrations. Thus, its storage poses a safety concern and its release is to be avoided. Moreover, ammonia is a poison to the anode of PEM fuel cells [5]. Thus, high conversion of ammonia should be achieved with minimal breakthrough in the hydrogen product stream.

The catalytic decomposition of NH_3 has been extensively studied on a number of different catalysts including metals, alloys, and nitrides [14,15]. Most of the studies were carried out in order to gain insights into the NH_3 synthesis process, but in recent years the focus has shifted to generation of H_2 [16]. The mechanism of NH_3 decomposition on the different catalysts has been classified into two forms [17,18]. At high temperatures and low H_2 partial pressures the rate is only dependent on NH_3 partial pressure and is not inhibited by the presence of H_2. This type of model is referred to as the "Tamaru model" and the rate expression can be of the form in Eq. (2a) or (2b):

$$\gamma = \frac{kKP_{NH_3}}{1 + KP_{NH_3}} \tag{2a}$$

$$\gamma = \frac{kKP^2_{NH_3}}{1 + KP^2_{NH_3}} \tag{2b}$$

where k is a rate constant and K is an adsorption equilibrium constant. At low temperatures and high H_2 partial pressures the rate is inhibited by the presence of H_2. This is referred to as the "Temkin-Pyzhev model" in which the rate is expressed as Eq. (3a) or (3b):

$$\gamma = k\left(\frac{P^2_{NH_3}}{P^3_{H_2}}\right)^{\beta} \tag{3a}$$

$$\gamma = \frac{k(KP_{NH_3})^2}{(KP_{NH_3} + P^{3/2}_{H_2})^2} \tag{3b}$$

Loeffler et al. [19,20] reported experimental data which clearly indicated a transition from Temkin-Pyzhev mechanism to the Tamaru mechanism on Pt catalyst. The temperature at which this transition occurred depended on the partial pressure of H_2. Chellapa et al. [21] carried out NH_3 decomposition on Ni-Pt/Al_2O_3 catalyst between 520 and 690 °C. Statistical analysis of the data obtained showed that NH_3 partial pressure was the only significant concentration variable. But they reported that the data between 520 and 560 °C could be fit well with the Temkin-Pyzhev type model utilizing a reaction order of −1 for H_2. Zhang et al. [22] carried out NH_3 decomposition on Ni nanoparticles of varying crystallite sizes on Al_2O_3 with varying concentrations of a La promoter at temperatures of 460–540 °C. The experimental data obtained fit very well to a Temkin-Pyzhev model with β values between 0.159 and 0.24 (Eq. (3a)).

For cases where the decomposition of NH_3 is inhibited by presence of H_2, at high conversions the rate decline due to declining ammonia concentration is exasperated by the increase in hydrogen concentration. Thus, the in situ removal of the hydrogen product may be beneficial from a kinetic standpoint, not unlike the thermodynamic benefit afforded by the removal of hydrogen during an equilibrium-limited dehydrogenation reaction.

The studies of catalytic decomposition of pure anhydrous ammonia in membrane reactors have been rarely reported. Most studies concentrated on developing catalysts for ammonia decomposition or generation of H_2 from ammonia in packed-bed reactors [23,24]. The development of a membrane reactor with planar configuration (Pd/Ag alloy) was reported by Vencill et al. and tests revealed a H_2 recovery of ~80–90% [25]. The device was operated for about 50 h and produced H_2 at a rate approaching 1 std. l/min at 600 °C with volumetric H_2 productivities varying from 1.7 to 2.7 mol/m^3 s. The other reported membrane reactor studies involved removal of ammonia from coal-derived synthesis gas which has ~0.3 mol% of ammonia [26–28]. Zhang et al. [29] carried out a membrane reactor study using Ni catalyst for NH_3 decomposition. The removal of H_2 significantly enhanced the conversion of NH_3. However, the performance of the membrane under reaction conditions was reported to be very poor as compared to permeation performance with pure gases. They suggested carrying out the reaction separately and then passing the resultant gas mixture through the membrane permeator. In this configuration approximately 2.4 mol/m^2/h of a 99.96% pure H_2 permeate stream was obtained at 77% recovery.

A number of studies have focused on the effects of nitrogen and ammonia on the Pd-membrane performance. Sakamoto et al. [30] separately tested the effect of 10% N_2 in H_2 and 10% NH_3 in H_2 on various Pd alloys. They measured the reduction in hydrogen flux through the membranes (as compared to the flux at pure hydrogen flow conditions) at temperatures between 250 and 450 °C and retentate pressures of 400 and 667 kPa. For pure Pd, the reduction percentage decreased linearly with temperature and had nearly the same values for both the nitrogen and ammonia case. At 300 °C the reduction was approximately 7% but dropped to zero at 450 °C. XPS analysis of the surface of a membrane which displayed a reduction in flux revealed an extra N1s peak as compared to the fresh membrane (for both the nitrogen and ammonia cases). The authors attributed the flux decrease to a decrease in effective area for hydrogen dissociation by the adsorption of nitrogen species on the Pd surface. In another study, Zhang et al. [29] measured a decrease of approximately 10% in hydrogen flux but no change in permeate purity when 55,840 ppm of ammonia was introduced into a 3:1 mixture of H_2:N_2 at 500 °C and a transmembrane pressure drop of 4 atm. Wilhite et al. [31] observed no change in the hydrogen flux of a pure Pd micromembrane at 350 °C and a transmembrane pressure of 9.6 kPa when they changed the inlet from a 10% H_2 in argon mixture to a 4% NH_3/10% H_2/90% Ar mixture.

The effect of concentration polarization due to the presence of a non-H_2 species on the retentate side has been well studied and has been shown to reduce the performance of the membrane [32–34]. For a 5 μm Pd composite membrane with an ideal H_2/N_2 separation factor of ~1000, Nair and Harold [34] compared the hydrogen and nitrogen fluxes through the membrane when pure gases are used and when H_2/N_2 mixtures are used. At 358 °C, a 10% N_2 in H_2 mixture resulted in a decrease of hydrogen flux by 30% and an increase of nitrogen flux by a factor of 7.

The objective of this study is to investigate the performance of a single fiber Pd-membrane reactor for the generation, separation and purification of hydrogen from ammonia. We report permeation, reaction and separation results for both a conventional top-layer Pd and a nanopore Pd membrane, both supported on porous alumina hollow fibers. We compare the packed-bed membrane reactor (PBMR) data to a conventional packed-bed reactor (PBR). The PBMR performance data are analyzed with a two-dimensional packed-bed membrane reactor model which utilizes the permeation and PBR data to estimate key permeation and reaction parameters. Finally, the PBMR model is used to elucidate the trends and to identify ways to improve reactor productivity for scale-up.

2. Experimental

2.1. Membrane synthesis

Two types of supported Pd membranes were synthesized for the current study; a top-layer Pd/α-Al_2O_3 membrane and a Pd/γ-Al_2O_3/α-Al_2O_3 nanopore membrane. The details of the syntheses follow from procedures described in previous studies [13,35]. We highlight the procedures here.

The differences in the procedures for synthesizing conventional top-layer and nanopore Pd membranes are shown in Fig. 1. The conventional membrane synthesis technique involved sequential sensitization and activation steps in which Pd nuclei were deposited onto the α-Al_2O_3 hollow fiber support. The deposition of Pd was then carried out using a multi-fiber ELP apparatus. In the Pd nanopore membrane synthesis, a layer of γ-Al_2O_3 was first deposited onto the α-Al_2O_3 surface followed by the sensitization/nucleation step. Another layer of γ-Al_2O_3 was then deposited on the nucleated surface, which ensured that in the subsequent ELP step the Pd deposition would occur in the pores of the second γ-Al_2O_3 layer. Table 1 gives a comparison of the conventional top-layer and nanopore membranes which were synthesized and used in the present study. The effective 4 μm thickness of the Pd nanopore membrane is based on the actual amount of Pd deposited. That is, if the amount of Pd deposited on the Pd nanopore membrane was used to synthesize a top-layer membrane its Pd thickness would be 4 μm. A fraction of the Pd in the nanopore membrane was deposited in the pores of the second γ-Al_2O_3 layer. Thus, the actual hydrogen diffusional distance through the Pd on the surface and within the pores membrane was approximately 6 μm.

The α-Al_2O_3 hollow fiber ceramic supports used in this study had a uniform composition and morphology (0.15 μm nominal pore diameter) and dimensions of 1 mm I.D., 2 mm O.D., length of 30.5 cm (supplied by Ceparation®, Helmond, the Netherlands). Before use, the fiber supports were rinsed with isopropyl alcohol and de-ionized water, dried in an oven at 120 °C for 12 h, then calcined at 600–800 °C in a box furnace for 3 h at a rate of 1 °C/min.

The γ-Al_2O_3 layers were deposited by slip casting a boehmite sol on the α-Al_2O_3 surface. A range of alumina loadings could be achieved by multiple dip coating, drying, and calcination cycles. Calcination was carried out at 450 °C for 3–4 h. The resulting top-layer of γ-Al_2O_3 afforded a smoother surface because of the smaller pore size (5–15 nm pore diameter) than the underlying α-Al_2O_3 fiber. Moreover, the nanoporous γ-Al_2O_3 film ensured dense and uniform population of nucleation sites for Pd.

The bath compositions for the sensitization, activation and ELP steps are provided in Table 2. The nucleation step consisted of alternate dipping in the sensitization and activation baths with intermediate dipping in de-ionized water. ELP was carried out in a

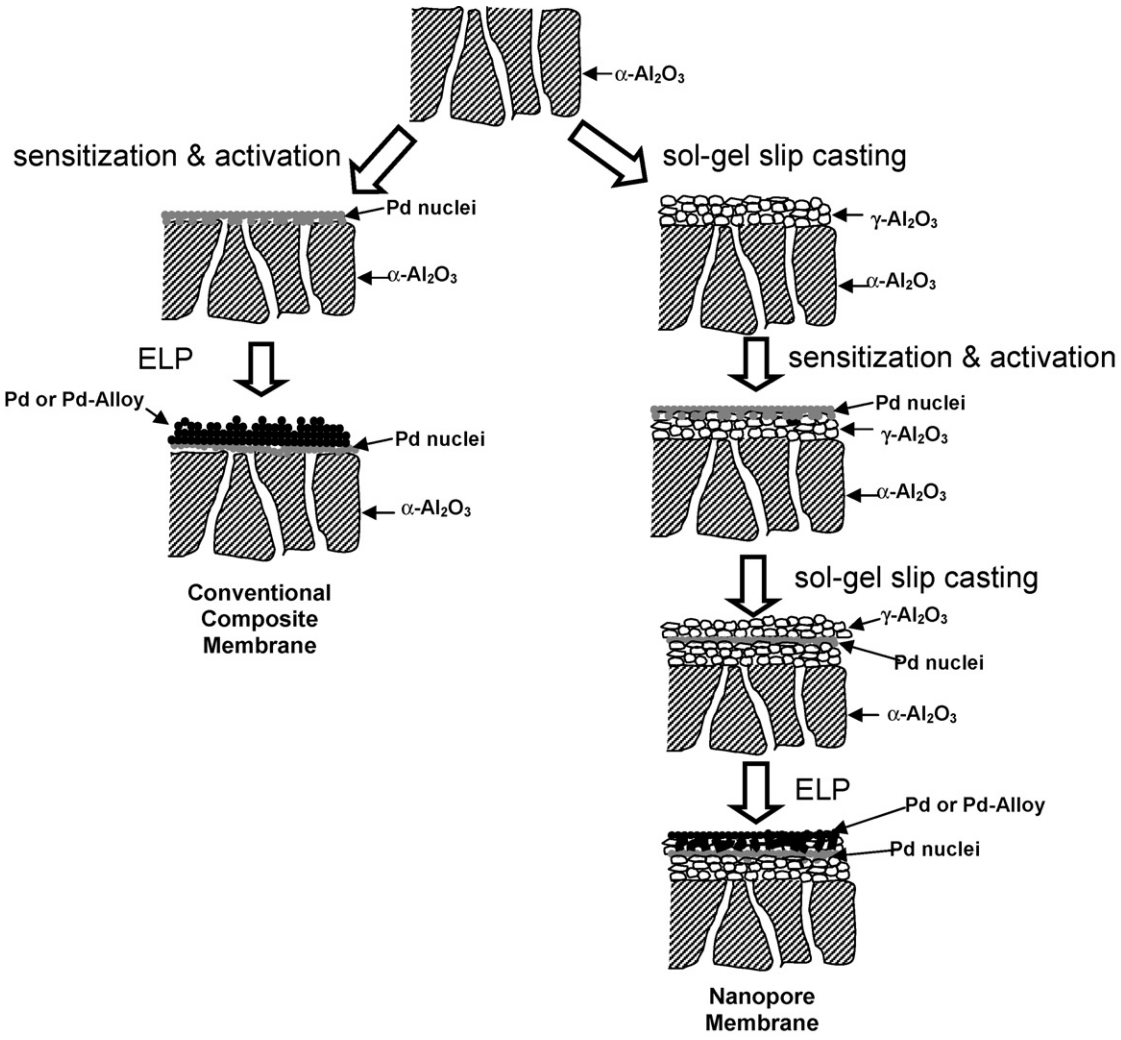

Fig. 1. Comparison of synthesis methods for conventional top-layer and nanopore Pd membranes.

Table 1
Comparison of the Pd top-layer and Pd nanopore membrane properties

Membrane type	Composite structure	Pd loading (g Pd/m^2 fiber)	Equivalent Pd thickness (μm)
Pd top layer	Pd/α-Al_2O_3	159	13
Pd nanopore	Pd-γ-Al_2O_3 (2 μm)/Pd nuclei/γ-Al_2O_3/α-Al_2O_3 (4 μm)	48	4

circulating multi-fiber apparatus. The Pd layer thickness was monitored in situ using a quartz crystal microbalance (Maxtek® PM-700 series) which was interfaced with a PC. The coated fibers were then rinsed with de-ionized water and kept in an oven at 120 °C. Before permeation with H_2 the membranes were reduced at 370 °C for 2–3 h in pure H_2 stream. A comparison of the two membranes used in this study is listed in Table 2.

2.2. Permeation studies

Detailed descriptions and schematics of the permeation system and single fiber permeation device have been provided previously [13,35]. The permeation system consisted of a tube furnace (Lindberg/Blue®) with temperature controller. The permeation device including the cell and preheat section was positioned within the insulated tube. Permeation gases (N_2 and H_2 in this study) were metered by mass flow controllers (Brooks-5850®). The exit streams from the mass flow controllers were connected to a static mixer and the resulting gas mixture flowed to a preheat section. The retentate pressure was controlled between 1 and 5 bar (absolute) using a back pressure regulator (US-gauge®) connected to the retentate effluent tube. The permeate side was open to the atmosphere through a bubble flow meter (Optiflow-520® or a capillary flow meter). All the inlet flow rates, pressures, and temperatures were logged into a PC using LABTECH® software. The single fiber permeation apparatus was essentially isothermal based on measurements from multiple thermocouples under flow conditions.

The permeation cell contained a single fiber. Graphite ferrules (Chromatography Research Supplies, Inc.) were used to seal the hollow fiber ends using modified Swagelok® fittings. One end of the fiber lumen was closed with a blank graphite ferrule and the other end was kept open through which the permeate was removed and sent to the bubble flow meter. The permeation results are reported in terms of H_2 transmembrane flux (mol H_2/m^2 s) and ideal H_2/N_2 separation factor (α). These measurements were carried out using pure H_2 and N_2 gases (Matheson Tri-Gas, UHP grade). In all experiments the permeate side was maintained at atmospheric pressure.

2.3. Ammonia decomposition in packed-bed reactor

The experimental set-up for ammonia decomposition reaction in a packed-bed reactor and packed-bed membrane reactor was similar to the permeation cell. The feed system comprised anhydrous ammonia (Matheson Trigas®, UHP grade) of 99.995% purity contained in a high pressure cylinder. The gaseous ammonia was metered through a mass flow controller (MKS-14709A®). The composition of all gases exiting the PBR and/or PBMR was measured with a gas chromatograph (Agilent-6890N®) equipped with a thermal conductivity detector (TCD). The operation and flow measurements were similar to that for the aforementioned permeation apparatus. The mass balances close within 10% for all the reactor experiments.

A schematic of the reactor is shown in Fig. 2. The catalyst used was a 70 wt% Ni supported on γ-Al_2O_3 and consisted of particles of nominal 1.4 mm particle diameter and bulk density of 0.91 g/cm^3 (supplied by Chemtron®). The PBR consisted of a stainless steel pipe 1.52 cm in inner diameter and 16.5 cm in length. The PBMR consisted of a similar stainless steel pipe within which the Pd coated fiber membrane was positioned coaxially. The length of the membrane was 15.6 cm for the conventional membrane and 12.7 cm for the nanopore membrane. The weight of the catalyst was 36 g in the PBR and 29 g in the PBMR.

The PBR and PBMR experiments were carried out at 500 and 600 °C with total catalyst-side pressures varying from 1 to 5 bar (absolute). The reactor was operated under essentially isothermal conditions confirmed by several thermocouple measurements. In the PBMR experiments the permeate side was open to the atmosphere through the GC or bubble flow meter and hence was only slightly above atmospheric pressure. The ammonia feed was varied from 30 to 700 sccm to span a range of space velocities. In all experiments the feed to the reactor was pure anhydrous ammonia. The reactor effluent (or retentate in the case of the PBMR) was vented to the vacuum hood after passing through the gas chromatograph and/or the bubble flow meter. All the flow lines and pressure gauges including back pressure regulator and valves were made of stainless steel to ensure compatibility with ammonia.

The PBMR data were used to calculate several key performance metrics besides the conversion of ammonia. The H_2 productivity (Π_{H_2}) (or membrane reactor space–time yield) is defined as molar flow rate of the permeate hydrogen product per unit reactor volume (mol permeate H_2/m^3 s). The fractional H_2 utilization (Y_{H_2}) is defined as fraction of H_2 fed into reactor (in the form of NH_3) that is recovered as permeate H_2:

$$\Pi_{H_2} = \frac{F_{H_2}^{perm}}{V_r} \tag{4}$$

$$Y_{H_2} = \frac{F_{H_2}^{perm}}{1.5 \times F_{NH_3}^{0}} \tag{5}$$

Table 2
Bath compositions for sensitization, activation and electroless plating used for the synthesis of the top-layer and nanopore membranes

Sensitization solution		Activation solution	
$SnCl_2$	1.2 g/l	$PdCl_2$	0.1 g/l
HCl	0.2N	HCl	0.2N
Electroless plating (ELP) bath compositions for Pd plating			
$PdCl_2$			5 g/l
NH_4OH (29.5 wt%)			600 ml/l
EDTA.2NA			40 g/l
N_2H_4 (1 M)			10 ml/l

3. Reactor model development

A two-dimensional, pseudo-homogeneous reactor model was utilized to simulate ammonia decomposition in the PBR and PBMR. On the retentate side the main model equations for each of the three species (NH_3, N_2, H_2) is of the dimensionless form

$$\frac{\partial(\nu' x_i^{ret})}{\partial Z} - \frac{1}{Pe_{i,r}'}\frac{1}{\xi}\frac{\partial}{\partial \xi}\left(\xi \frac{\partial x_i^{ret}}{\partial \xi}\right) = \vartheta_i Da \gamma' \tag{6a}$$

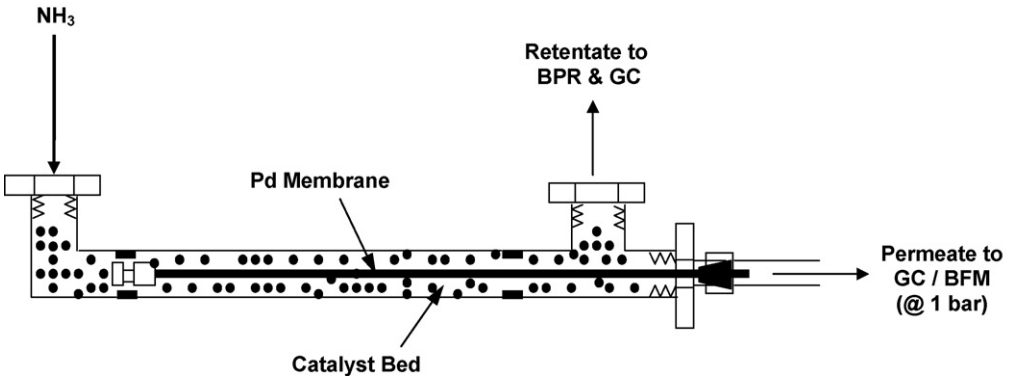

Fig. 2. Diagram of the single fiber membrane reactor used for NH_3 decomposition.

The first term on the left hand side represents the mass transfer due to axial convection, the second term is the mass transfer due to radial dispersion and the term on the right hand side is the reaction term. *Da* is the Damkohler number and $Pe_{i,r'}$ is the modified transverse Peclet number which is explained further in section 5. ϑ_i is the stoichiometric coefficient for the *i*th component ($\vartheta_{NH_3} = -1$, $\vartheta_{H_2} = 1.5$, $\vartheta_{N_2} = 0.5$). The overall mass balance equation is:

$$x_{NH_3}^{ret} + x_{H_2}^{ret} + x_{N_2}^{ret} = 1 \tag{6b}$$

The boundary conditions are

$$@Z = 0, \quad x_{NH_3}^{ret} = 1, \quad x_{N_2}^{ret} = x_{H_2}^{ret} = 0, \quad \nu' = 1 \tag{7a}$$

$$@\xi = 1, \quad \frac{\partial x_{NH_3}^{ret}}{\partial \xi} = \frac{\partial x_{H_2}^{ret}}{\partial \xi} = \frac{\partial x_{N_2}^{ret}}{\partial \xi} = 0 \tag{7b}$$

$$@\xi = \frac{r_m}{R}, \quad \frac{\partial x_{NH_3}^{ret}}{\partial \xi} = \frac{\partial x_{N_2}^{ret}}{\partial \xi} = 0 \tag{7c}$$

$$\text{For PBR } @\xi = \frac{r_m}{R}, \quad \frac{\partial x_{H_2}^{ret}}{\partial \xi} = 0 \tag{7d}$$

$$\text{For PBMR } @\xi = \frac{r_m}{R}, \quad \frac{\partial x_{H_2}^{ret}}{\partial \xi} = \phi[(x_{H_2}^{ret})^{0.5} - (x_{H_2}^{perm})^{0.5}] \tag{7e}$$

In Eq. (7e), ϕ is the ratio of characteristic times of radial dispersion and permeation. This term is explained in further detail in Section 5. The solution of the four equations ((6a) and (6b)) gives the composition and velocity of the retentate side.

The main assumptions of the model are:

- Mass transport limitations are neglected at the level of the supported Ni catalyst. By using different catalyst bed lengths and varying gas velocities (in order to keep space velocities constant), it was verified that there are no external mass transfer limitations. The value of the Weisz-Prater parameter [36] was estimated to be ~0.3 for the case of 600 °C and 1 bar retentate pressure in the PBR. Thus, this assumption is reasonable.
- The inlet velocity profile was assumed to be flat in the radial direction (plug flow). End effects were also ignored.
- Both the PBR and PBMR were assumed to be isothermal. This was initially verified experimentally by placing thermocouples at 3 different positions along the length of the reactor. The difference in temperatures for all furnace temperatures and flow rates was less than 5 °C.
- The membrane was assumed perfectly permselective and therefore the permeate side comprised H_2 product at 1 bar total pressure.
- Ammonia and nitrogen are assumed to not cause a decrease in membrane performance due to surface poisoning. XPS analysis of the aged and fresh membrane did not reveal any major changes in surface species and concentrations. The study carried out by Sakamoto et al. [30] also confirmed that there is no evidence of surface poisoning by nitrogen and ammonia above 450 °C.

The trends observed in the PBR and PBMR results (discussed in the next two sections) indicated the form of the rate expression which was valid for the current study. Kinetic parameters contained in the rate expression were estimated from a fit of the PBR data as described below.

The effective radial dispersion coefficient (D_{er}) was determined using the correlation of Gunn [37] for spherical particles in a fixed bed. For a given component the radial dispersion coefficient can be determined using Eqs. (8) and (9) below. Eq. (8) considers the contribution of both the axial convection and molecular diffusion to the radial dispersion coefficient:

$$\frac{\varepsilon D_r}{\nu d} = \frac{1}{40 - 29\exp(-7/N_{Re})} + \frac{\varepsilon}{\tau N_{Re} Sc} \tag{8}$$

$$D_{er} = \frac{\varepsilon D_r}{\tau} \tag{9}$$

where ε and τ are the bed porosity and tortuosity. All of the parameters are defined in the list of notation.

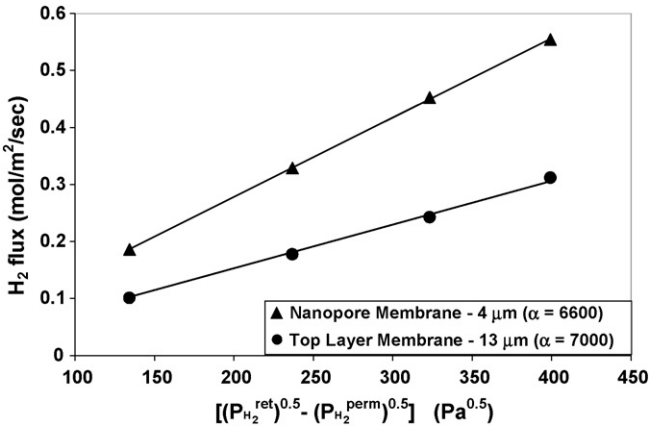

Fig. 3. Comparison of permeation characteristics between the Pd top-layer and Pd nanopore membranes at 500 °C. The points are the experimental data and the lines are the trendlines.

Table 3
Estimated permeance parameters for the top-layer and nanopore Pd membranes

Pd-membrane type	Permeance pre-exponential factor, q_o (mol/m^2 s Pa$^{0.5}$)	Permeance activation energy, E_H (kJ/mol)
Top layer	5.562	22.32
Nanopore	1.523	7.95

4. Results

4.1. Permeation

The permeation features of the top-layer and nanopore membranes were measured in the permeation apparatus. Fig. 3 compares the pure gas permeation results for the 13 μm top-layer and the 4 μm nanopore Pd membranes at 500 °C (the points represent the experimental data and the lines indicate the trends). The measured hydrogen flux was determined to be a linear function of the difference of the square root of the H_2 partial pressure on the retentate and permeate sides. This indicates that the hydrogen permeation follows Sieverts' flux law for which the diffusion of atomic hydrogen through Pd is rate limiting, i.e.

$$J_{H_2} = q(T)\left[\sqrt{p_{H_2}^{ret}} - \sqrt{p_{H_2}^{perm}}\right] = q_o \exp\left(-\frac{E_H}{\Re T}\right)\left[\sqrt{p_{H_2}^{ret}} - \sqrt{p_{H_2}^{perm}}\right] \quad (10)$$

where J_{H_2} is the transmembrane flux and $q(T)$ is the permeance. Flux data were obtained from 400 to 600 °C, from which q_o and E_H were estimated for both membranes. Table 3 provides the parameter estimates for the top-layer and nanopore membranes. For a fixed retentate pressure the H_2 flux through the Pd nanopore membrane was about twice that through the Pd top-layer membrane. [Remark: The estimated Pd thickness of 6 μm is about half of the top-layer membrane.] The H_2 flux through the unplated membrane support was also measured. At 500 °C and 5 bar retentate pressure the H_2 flux through the nanopore membrane was 2.5 mol/m^2/s before Pd plating and 0.56 mol/m^2/s after Pd plating. The ideal H_2/N_2 separation factor (α) at 500 °C for the top-layer and nanopore membranes was 7000 and 6600, respectively. Over the course of this study the permeation characteristics remained nearly constant.

4.2. Packed-bed reactor

The conversion of ammonia in the packed-bed reactor was measured as a function of the space velocity for several combinations of temperature and total pressure. The dependence of the NH_3 conversion on the gas hourly space velocity (GHSV; scc/h g cat) is shown in Fig. 4 at 500 and 600 °C for several total pressures. (The experimental measurements are the points in the figure while the curves are model predictions described in more detail in the next section.) The conversion decreased with an increase in space velocity for all temperatures and pressures, although the decrease was more pronounced at 500 °C than at 600 °C. For a given temperature and space velocity the NH_3 conversion moderately decreased with an increase in total pressure.

4.3. Packed-bed membrane reactor

A direct comparison of the PBR and the PBMR reveals the effect of hydrogen removal from the reaction zone. Fig. 5 compares the NH_3 conversions for the PBR to the PBMR containing the top-layer membrane while Fig. 6 shows the corresponding comparison for the PBMR containing the Pd nanopore membrane. In spite of the large differences in the pure H_2 permeance of the two membrane types, there was only a negligible difference in the ammonia conversion dependence on the space velocity at the various temperature and retentate pressures. For both membrane types the NH_3 conversion for the PBMR was higher than for the PBR at all temperatures and pressures. For both PBMR cases the dependence of conversion on the catalyst-side (retentate) total pressure was more complex than the pressure dependence observed for the PBR. At the lower temperature of 500 °C, the ammonia conversion increased with the retentate pressure for all space velocities below a critical value (about 400 cm^3/h g cat). The conversion versus retentate pressure trend reversed at space velocities exceeding this critical value. The PBMR data at 600 °C were too close to 100% to discern a similar trend.

Figs. 7 and 8 show the PBMR data in the form of H_2 volume productivity (Π_{H_2}) and utilization (Y_{H_2}) for the Pd top-layer and Pd nanopore membranes, respectively. The results are similar for both membrane types. The H_2 utilization decreased monotonically with space velocity. The productivity exhibited

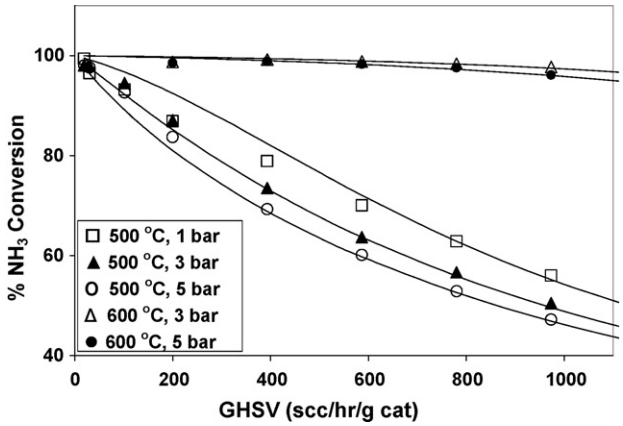

Fig. 4. NH_3 conversions in PBR as a function of the space velocity for several combinations of temperature and retentate pressures. The points are the experimental data while the curves are the model predictions.

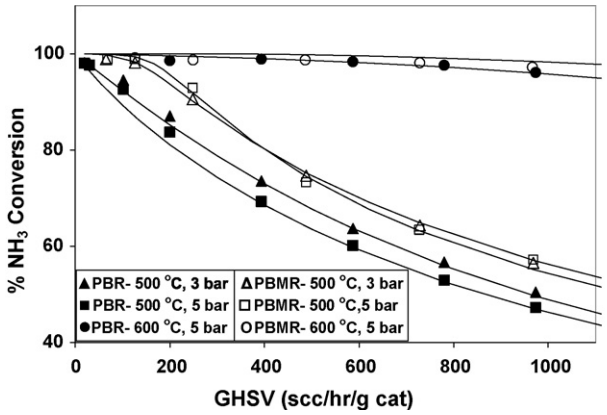

Fig. 5. Comparison of NH_3 conversions obtained in the PBR and PBMR containing the Pd top-layer membrane. The points are the experimental data, the dashed lines are the PBR model results and the solid lines are the PBMR model results.

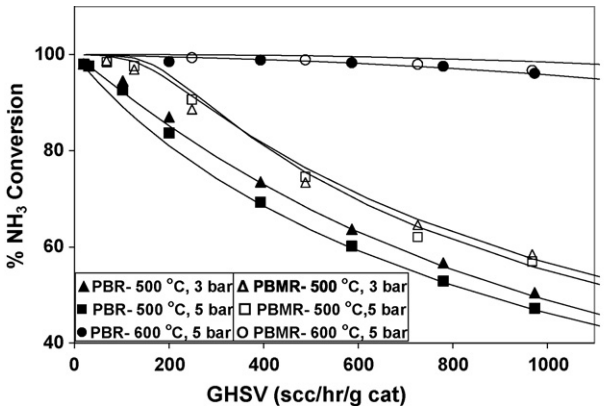

Fig. 6. Comparison of NH_3 conversions obtained in the PBR and PBMR containing the Pd nanopore membrane. The points are the experimental data, the dashed lines are the PBR model results and the solid lines are the PBMR model results.

a maximum at an intermediate space velocity for the 500 °C experiments while at 600 °C and 5 bar retentate total pressure the productivity did not exhibit a maximum for the space velocities employed. Both the utilization and productivity increased with temperature and retentate pressure. As space velocities approached a low value, the productivity approached zero while the H_2 utilizations approached a limiting value in the range of 80–90%; the limiting value increased with retentate pressure. The experiments determined that the productivity maximum occurred at an intermediate hydrogen utilization.

Finally, in Fig. 9 the purity of the H_2-rich permeate stream is reported as a function of the space velocity. The H_2 purity in all cases exceeded 99.2% and did not exhibit a discernible dependence on the space velocity, temperature or retentate pressure.

5. Analysis and discussion

The experimental findings show that the high-purity hydrogen can be produced during high temperature catalytic decomposition of ammonia in a Pd-based membrane reactor. While the reactor volume productivity and hydrogen purity are not at the desired levels of 50 mol/m^3 s and 99.99%, the results reported here are

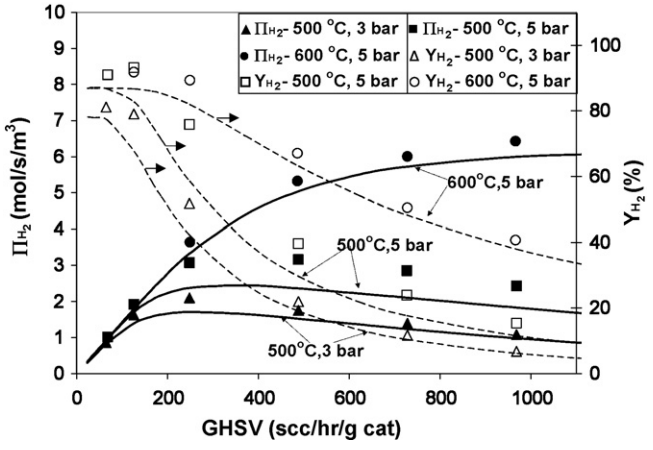

Fig. 7. Permeate hydrogen volume productivity and hydrogen utilization as a function of the space velocity for the PBMR containing the conventional top-layer Pd membrane, for three different temperature and retentate total pressure conditions. The points are the experimental data, the dashed lines are the model predictions for H_2 utilization and the solid lines are model predictions for H_2 productivities.

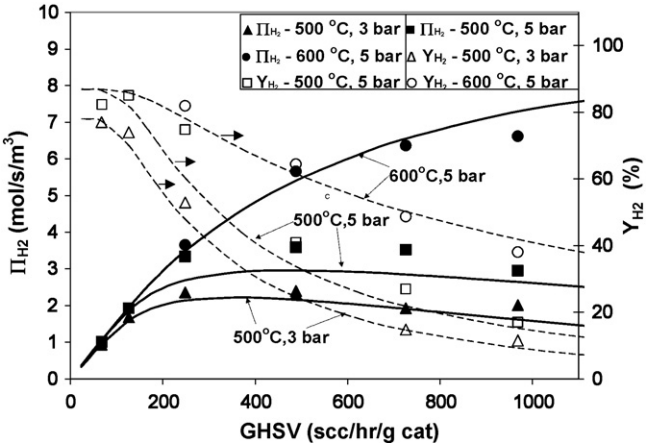

Fig. 8. Permeate hydrogen volume productivity and hydrogen utilization as a function of the space velocity for the PBMR containing the nanopore Pd membrane, for three different temperature and retentate total pressure conditions. The points are the experimental data, the dashed lines are the model predictions for H_2 utilization and the solid lines are model predictions for H_2 productivities.

encouraging. The advantage of hydrogen removal, as we show below, is the result of the suppression of a kinetic rate limitation caused by hydrogen. In this section we utilize the models of the PBR and PBMR to interpret the results and to investigate membrane reactor design modifications to further increase the productivity.

Thermodynamic calculations show that at temperatures of 500 °C and higher and total pressures of 5 bars and below, equilibrium limitations are negligible for the decomposition of ammonia, i.e. the reaction is essentially irreversible. With this in mind, the results obtained for the packed-bed reactor must be interpreted in terms of kinetic/transport rather than thermodynamic factors. For example, Fig. 4 shows that the conversion decreased with an increase in the total pressure at a fixed temperature and flow rate. We attribute this trend to the inhibition of ammonia decomposition by product hydrogen. As described earlier, the Temkin-Pyzhev type of mechanism infers such an inhibitory effect (Eqs. (3a) and (3b)).

Following this argument, we carried out a fit of the integral PBR data in Fig. 4. Without showing the details here, the following expressions were obtained for kinetic constants k and K contained

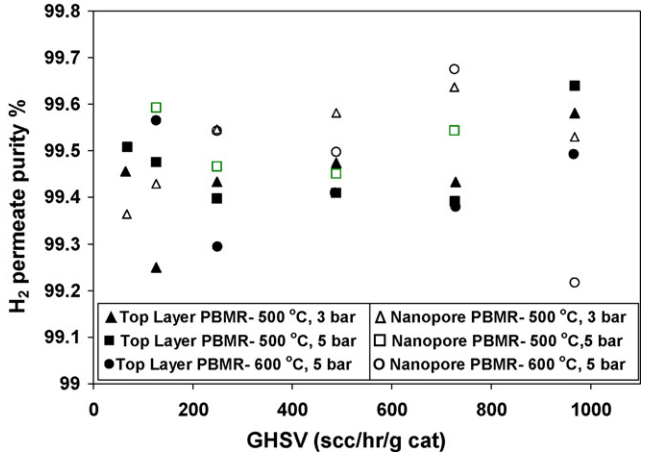

Fig. 9. Purity of H_2 in the permeate stream of the PBMR for both membranes and several operating conditions.

in the rate expression (3b):

$$k\,(\mathrm{mol/m^3/s}) = 3.17 \times 10^6 \exp\left[\frac{-80.39\,(\mathrm{kJ})}{\Re T}\right] \tag{11}$$

$$K\,(\mathrm{bar}^{0.5}) = 1.35 \times 10^6 \exp\left[\frac{-83.46\,(\mathrm{kJ})}{\Re T}\right] \tag{12}$$

While fitting a rate expression does not prove a mechanism, the trends do lend credence to product inhibition. Fig. 4 shows the prediction of the PBR data using these parameter values in the rate expression and solving the PBR reactor model at the various conditions (temperature, total pressure, feed flow rate). The model clearly does a good job of capturing the main trends in the conversion data. Notably, the inhibitory effect of total pressure on the conversion is predicted. Hence, the explanation for this trend is the inhibitory effect of the product hydrogen on the decomposition rate.

Simulations of the PBMR were carried out using the independent estimates of the permeance parameters for the Pd top-layer and Pd nanopore membranes (Table 3) and the kinetic parameters (Eqs. (11) and (12)). No other parameters were adjusted during this exercise. Figs. 5–8 compare the experimental data (points) to the model predictions (solid and dashed lines).

The dependence of the ammonia conversion on space velocity in the PBMR is captured well by the membrane reactor model (Figs. 5 and 6). In particular, the model predicts the enhancement of the ammonia conversion. While the enhancement is limited to about a 10% absolute increase in the conversion, the simulations underscore the fact that the removal of hydrogen suppresses the inhibitory effect of hydrogen. The model even captures the subtle cross-over of the ammonia conversion for the 3 and 5 bar total pressure experiments at 500 °C. At space velocities lower than this point an increase in retentate pressure increases the conversion, exemplifying the positive impact of pressure on the driving force for hydrogen permeation. For space velocities beyond the cross-over point the PBMR has the same qualitative behavior of the conversion dependence on pressure as the PBR. Under these conditions the pressure has the same beneficial effect of increasing the driving force for hydrogen permeation, but the detrimental effects of reducing the rate of ammonia decomposition and reducing the radial transport (dispersion) flux of hydrogen. We return to this point below. Finally, the model also predicts the rather small difference in performance of the two membrane types, another point that we return to later.

The PBMR model simulations also predict the trends in the hydrogen volume productivity and utilization as a function of the space velocity in Figs. 7 and 8. The model predicts, as was observed experimentally, that the productivity exhibits a maximum at an intermediate space velocity while the utilization decreases monotonically with space velocity. These features were first described in a modeling study of methanol reforming by Harold et al. [6]. At low space velocity the conversion, in this case ammonia, approaches 100%. However, the production of hydrogen is limited by the supply (feed rate) of the hydrogen-containing reactant to the reactor. On the other hand, at high space velocities the conversion is low and the production of hydrogen is kinetically limited. As a result, insufficient hydrogen is generated in the reaction zone and the hydrogen partial pressure is inadequate. At intermediate space velocity the hydrogen partial pressure achieves a maximum value which leads to the productivity maximum.

At low space velocities, the ammonia conversion is nearly complete. Under these conditions the hydrogen utilization approaches a limiting value that depends only on the ratio of retentate total pressure to permeate H_2 partial pressure, $P_0/P^{\mathrm{perm}}_{H_2}$ [6]. At very low space velocity the hydrogen retentate partial pressure approaches the permeate pressure of hydrogen (i.e. $p^{\mathrm{ret}}_{H_2} = p^{\mathrm{perm}}_{H_2}$). Under these conditions the retentate molar flow rate of hydrogen is approximated by

$$(F^{\mathrm{ret}}_{H_2})_{z=L,\,x_{NH_3}\to 0} = x^{\mathrm{ret}}_{H_2}(F^{\mathrm{ret}}_{NH_3} + F^{\mathrm{ret}}_{H_2} + F^{\mathrm{ret}}_{N_2})_{z=L,\,x_{NH_3}\to 0} \tag{13}$$

$$(F^{\mathrm{ret}}_{H_2})_{z=L,\,x_{NH_3}\to 0} = \frac{P^{\mathrm{perm}}_{H_2}}{P_o}\left(F^{\mathrm{ret}}_{H_2} + \frac{F^0_{NH_3}}{2}\right)_{z=L,\,x_{NH_3}\to 0} \tag{14}$$

The limiting H_2 utilization can be written as

$$(Y_{H_2})_{\mathrm{GHSV}\to 0} = \frac{(F^{\mathrm{perm}}_{H_2})_{z=L,\,x_{NH_3}\to 0}}{1.5 \times F^0_{NH_3}} = \frac{1.5 \times F^0_{NH_3} - (F^{\mathrm{ret}}_{H_2})_{z=L,\,x_{NH_3}\to 0}}{1.5 \times F^0_{NH_3}} \tag{15}$$

which leads to the result

$$(Y_{H_2})_{\mathrm{GHSV}\to 0} = 1 - \frac{P^{\mathrm{perm}}_{H_2}/P_o}{3(1 - P^{\mathrm{perm}}_{H_2}/P_o)} \tag{16}$$

For example, for a permeate pressure of 1 bar and a retentate pressure of 5 bar, the percent utilization is 91.67%. This is close to the experimental value of 90.8% for the conventional membrane PBMR at 500 °C and 5 bar retentate pressure.

The productivities achieved in the experiments were well below the target of 50 mol H_2/m^3 s. While the percent hydrogen utilization approached 90%, these were achieved at space velocities that gave rather low productivity (i.e. on the order of 1–2 mol H_2/m^3 s). It is of interest to understand the factors limiting the productivity. Of particular importance is the identification of the process limiting the hydrogen utilization at high ammonia conversion. For example, at 600 °C, 5 bar retentate pressure, and space velocity of 1000 scc/h g cat, the ammonia conversion is over 95% but only about 40% of the hydrogen fed to the reactor as ammonia is recovered as H_2 on the permeate side.

To this end, it is instructive to estimate the characteristic times for the key processes of hydrogen permeation, radial dispersion, flow, and reaction. These are respectively defined as follows. The characteristic *flow time* is the ratio of the membrane length to linear interstitial velocity of the feed:

$$\tau_f = \frac{L}{v_0} \tag{17}$$

The characteristic *reaction time* is the ratio of the feed ammonia concentration (C^0) to the reference decomposition rate:

$$\tau_r = \frac{C^0}{r(C^0)} \tag{18}$$

The characteristic *permeation time* is the ratio of feed ammonia concentration to a reference volume productivity, the product of a reference flux ($J^0_{H_2}$) and the membrane area per unit reactor volume (S_m/V_r):

$$\tau_p = \frac{C^0 V_r}{J^0_{H_2} S_m} = \frac{C^0 V_r}{q(T^0)P_0^{0.5} S_m} \tag{19}$$

The characteristic *radial dispersion time* is the ratio of the square of the annular gap thickness to the radial dispersion coefficient of hydrogen:

$$\tau_d = \frac{(R - r_m)^2}{D_{H_2 er}} \tag{20}$$

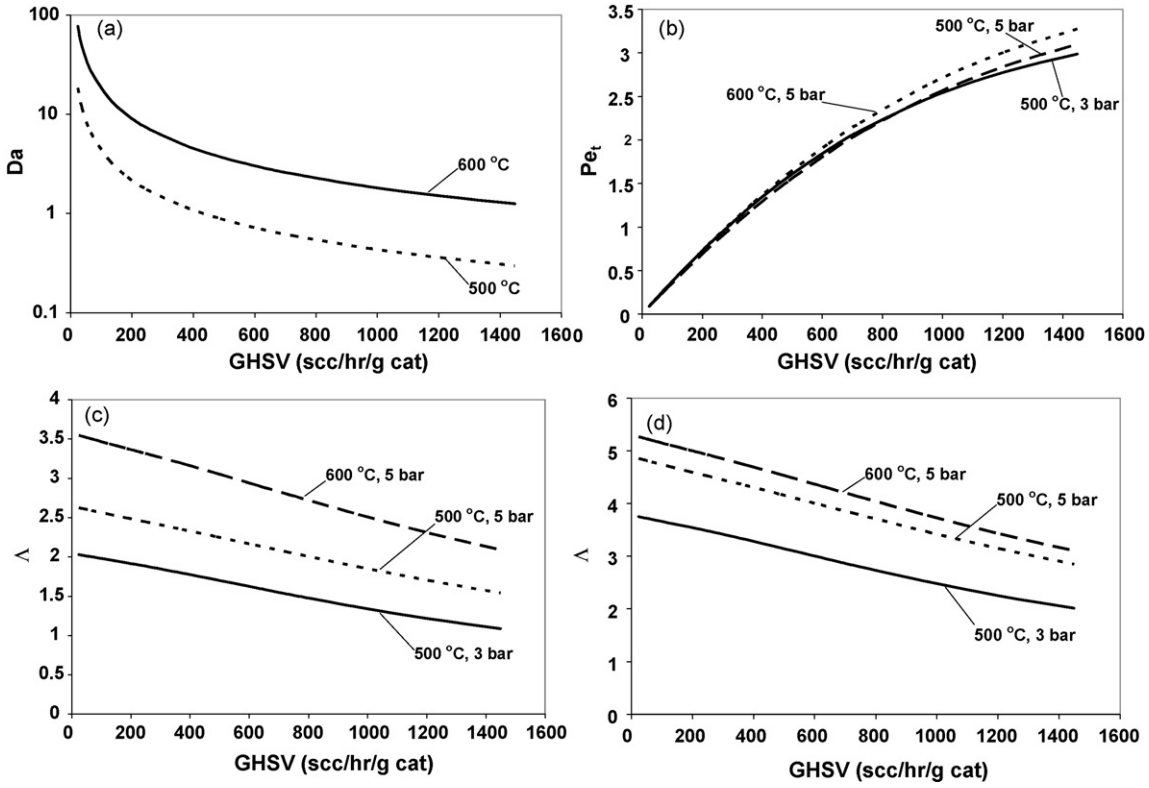

Fig. 10. Dependence of characteristic times on space velocity for different temperature and retentate total pressure combinations: (a) Da, (b) Pe_t, (c) Λ (top-layer membrane) and (d) Λ (nanopore membrane).

Using these characteristic time definitions, one can estimate key dimensionless parameters that are ratios of two characteristic times. Specifically, the Damkohler number is the ratio of the characteristic flow and reaction times:

$$Da = \frac{\tau_f}{\tau_r} \tag{21}$$

A high value of Da ($\gg 1$) is needed to achieve a high conversion. The transverse Peclet number is the ratio of the characteristic radial dispersion time to axial flow time:

$$Pe_t = \frac{\tau_d}{\tau_f} = Pe'_{H_2,r}\frac{(R - r_m)^2}{R^2} \tag{22}$$

If $Pe_t \gg 1$ then the radial dispersion is slower than the axial flow which means gas phase radial gradients are likely to be present. Finally, the ratio of the radial dispersion and permeation times is given by

$$\Lambda = \frac{\tau_d}{\tau_p} = \phi\frac{(R - r_m)^2}{R}\frac{S_m}{V_r} \tag{23}$$

If $\Lambda \gg 1$ then the radial dispersion time is much larger than the permeation time, which indicates that radial dispersion will limit permeate H_2 flux through the membrane.

How the characteristic time or ratio estimates depend on the operating conditions (flow rate, temperature, pressure) enables one to identify the rate limiting processes. These estimates are helpful in explaining the trends of the experiments and in optimizing the reactor for improved performance, Fig. 10a and b shows the dependence of Da and Pe_t (for H_2) on the space velocity for different combinations of temperature and retentate pressure. Fig. 10c and d shows the corresponding dependence of Λ on the space velocity for the top-layer and nanopore Pd membrane, respectively.

The dependence of the Damkohler number (Da; Eq. (21)) on the space velocity, shown in Fig. 10a, reveals the expected transition from a high conversion to moderate conversion state. At 600 °C and 5 bar Da exceeds 1 even up to a space velocity of 1500 scc/h g cat which explains the observed high ammonia conversion (Figs. 4–6). A drop in the temperature to 500 °C results in a nearly an order of magnitude decrease in Da (Fig. 10a). Under these conditions the conversion is more sensitive to a change in the space velocity and is below 50% at 1500 scc/h g cat (Figs. 4–6).

The dependence of the transverse Peclet number for H_2 (Pe_t; Eq. (22)) on the space velocity is shown in Fig. 10b reveals the importance of the radial dispersion. For all the conditions above a space velocity of 300 scc/h g cat Pe_t has a value greater than unity, which indicates that radial gradients play a role in the reactor behavior. The corresponding value of the parameter Λ will determine how steep the H_2 radial gradients actually are.

The dependence of ratio of the radial dispersion and permeation times (Λ; Eq. (23)) on the space velocity shown in Fig. 10c and d for the nanopore and top-layer membranes, respectively. The estimates reveal that the gas phase radial transport is definitely slower than permeation through the membrane (for both membrane types) under all tested conditions. Based on the values of Pe_t and Λ it is clear that the radial transport of H_2 in the gas phase is the rate limiting process. Due to the higher permeance of the nanopore membrane as compared to the conventional membrane PBMR, under similar conditions the value of Λ is larger for the nanopore PBMR (compare Fig. 10c. and d). This explains why there is not much difference in reactor productivity of top-layer and nanopore PBMRs even though the pure gas H_2 permeance of the nanopore membrane is twice that of the top-layer membrane.

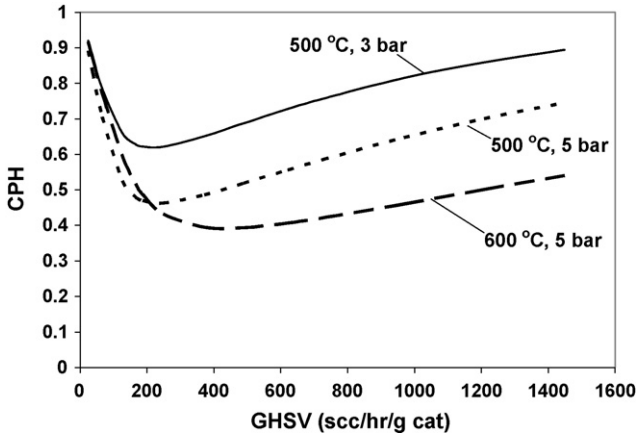

Fig. 11. Model CPH values in PBMR containing nanopore Pd membrane.

Another way of elucidating the radial transport limitations is through the use of the degree of concentration polarization for hydrogen (CPH), which is obtained using the results of the 2-D model. CPH is defined here as the ratio of the length-average H_2 concentration at the surface of the membrane to length-average H_2 concentration at the wall. The average is taken along the length of the reactor:

$$\mathrm{CPH} = \frac{\int_L C_{H_2}\,(\text{reactor wall})\,dz}{\int_L C_{H_2}\,(\text{Pd surface})\,dz} \tag{24}$$

A CPH of unity indicates that radial diffusion is sufficiently fast and is not limiting, as compared to the permeation through the membrane. The lower the value of CPH, the slower is the radial diffusion compared to the permeation through the membrane. Fig. 11 gives further evidence of the importance of radial diffusion and its role as the rate limiting step in the generation of high-purity H_2.

Fig. 12 shows the results of using a 1-D model in comparison to the 2-D model for the PBMR cases at 600 °C and 5 bar retentate pressure. In using the 1-D model we disregard the effect of radial diffusion and assume that this transport process is extremely fast. The results of the 1-D model can also be interpreted as a case in which the radial diffusivity has been artificially increased such that the CPH values are unity for all cases. In the 1-D case we see that not only are the productivities

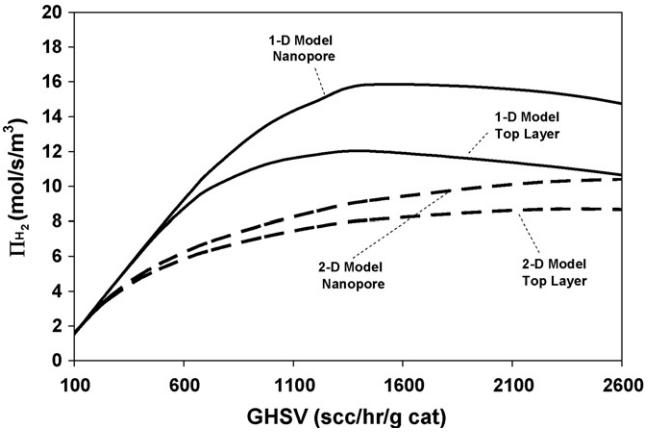

Fig. 12. Comparison of hydrogen volume productivity results for 1-D (solid lines) and 2-D (dashed lines) model predictions for nanopore and top-layer PBMRs at 600 °C and 5 bar retentate pressure.

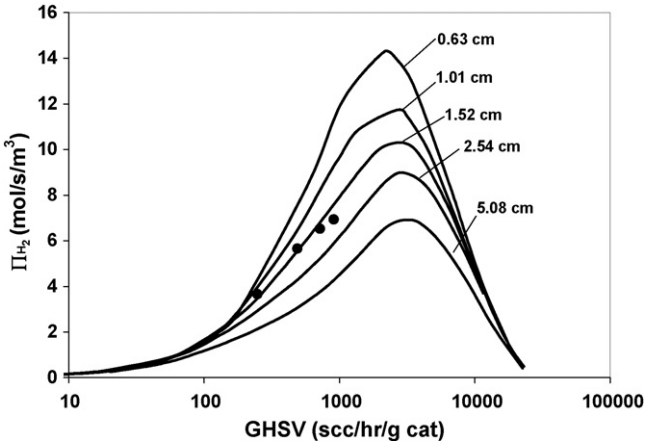

Fig. 13. Model H_2 productivities for various reactor and fiber diameters, keeping S_m/V_r constant (nanopore PBMR at 600 °C, 5 bar total retentate pressure). The points are the experimental data for the reactor diameter used in the study.

higher but now there is a definite difference in the results for the nanopore and conventional membrane PBMRs, as would have been expected based on difference in pure gas H_2 permeabilities of the membranes.

The average hydrogen permeate purity obtained was in the range 99.2–99.5% (Fig. 9). This is lower than the value that is expected from membranes with an ideal separation factor of 6000–7000 (at 500 °C). A combination of the following three factors could cause the decrease in the separation efficiency of the membrane under reaction conditions.

- Concentration polarization has the effect of decreasing the separation factor from the pure gas (ideal) separation factor [32–34]. Since the H_2/N_2 separation factor is the ratio of the hydrogen flux to the nitrogen flux through the membrane, a decrease in the hydrogen flux due to the concentration polarization effect will reduce the separation factor. To estimate the magnitude of the decrease, consider a hydrogen retentate pressure of 3 bar and permeate pressure 1 bar. If the CPH value is 0.6 (as in Fig. 11), the hydrogen flux will decrease by a factor of $\{(3 \times 0.6)^{0.5} - (1)^{0.5}\}/\{(3)^{0.5} - (1)^{0.5}\} = 0.47$, over the case when there is no concentration polarization. Similarly there will be an enhancement of the N_2 flux due to an increase in the concentration of nitrogen at the membrane surface. Both these factors would adversely affect the separation efficiency of the membrane.

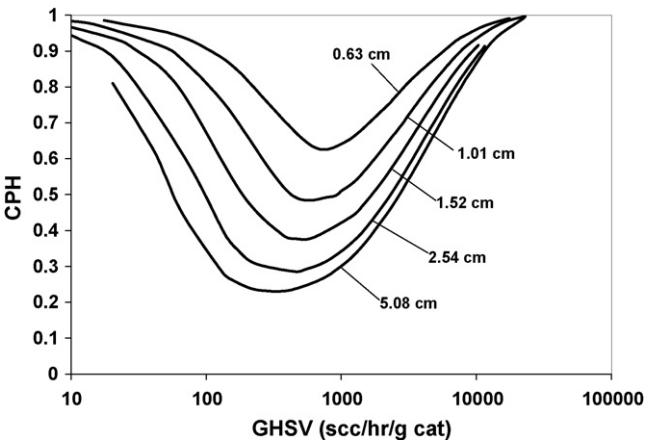

Fig. 14. Model CPH values for various reactor and fiber diameters, keeping S_m/V_r constant (nanopore PBMR at 600 C, 5 bar total retentate pressure).

- Ammonia, being a smaller molecule than nitrogen, should have a larger flux through the defects in the membrane (by a factor of 1.28), assuming the governing transport mechanism is Knudsen diffusion. This factor would be especially important in the initial section of the reactor, where ammonia is abundant, and when conversion is low.
- In the hydrogen rich atmosphere on the permeate side, the conversion of nitrogen to ammonia would be thermodynamically favored. This conversion may be catalyzed by the Pd or even the stainless steel reactor walls. Since one molecule of nitrogen would give two molecules of ammonia and also consume three molecules of hydrogen, this conversion would decrease the apparent separation efficiency. For example, if the actual permeate purity was 99.95% hydrogen (corresponding to a separation factor of 2000), and if the remaining 0.05% was only nitrogen, then complete conversion of the nitrogen to ammonia would decrease the permeate purity to $\{(99.95-(0.05\times 3))\}/\{(99.95-(0.05\times 3))+(0.05\times 2)\}=99.89\%$ (corresponding to a separation factor of 908). In all the experimental results in the current work the permeate impurity detected was only ammonia. The amount of nitrogen in the permeate was undetectable. These experimental results lend credence to this theory.

Since NH_3 is a poison for the PEM fuel cell, the permeate H_2 needs to be further treated before use in the fuel cell. Technologies for removing ammonia include adsorption onto zeolites or other catalyst materials like $Pt/BaO/Al_2O_3$ which can then be continuously or intermittently oxidized under the right conditions to give harmless products like N_2 and H_2O [38].

The 2-D model can also be used to evaluate different geometries and operating conditions in order to determine if the volume productivity can be increased from the levels observed experimentally. Figs. 13 and 14 show the results of some simulations in which the dimensions of the reactor and the membrane fiber were changed in order to study the effect of increasing/decreasing the characteristic radial diffusion time. In each case the diameter of the membrane was also varied such that the S_m/V_r ratio remained the same as for the experimental case. The reactor diameters selected were 0.63, 1.01, 1.52 (experimental value), 2.54 and 5.08 cm. The corresponding membrane diameters were 0.34, 0.89, 2, 5.5 and 22.2 mm. As can be seen from Fig. 14, the CPH values approaches unity as the reactor diameter is decreased. The corresponding reactor productivities increase for smaller reactor diameters and vice versa. Although some of the reactor and membrane diameters used in this simulation are impractical, these results show the importance of a good design of the PBMR.

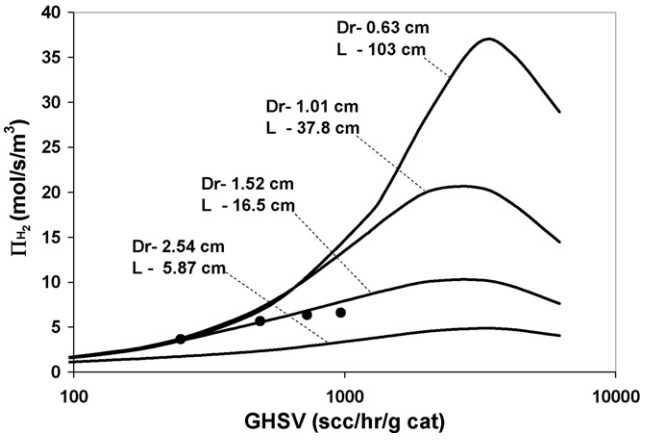

Fig. 15. Model H_2 productivities for various reactor diameters and lengths (fiber diameter kept constant at 2 mm). In each case the amount of catalyst is 29 g (nanopore PBMR at 600 °C, 5 bar total retentate pressure). The points are the experimental data for the reactor diameter used in the study.

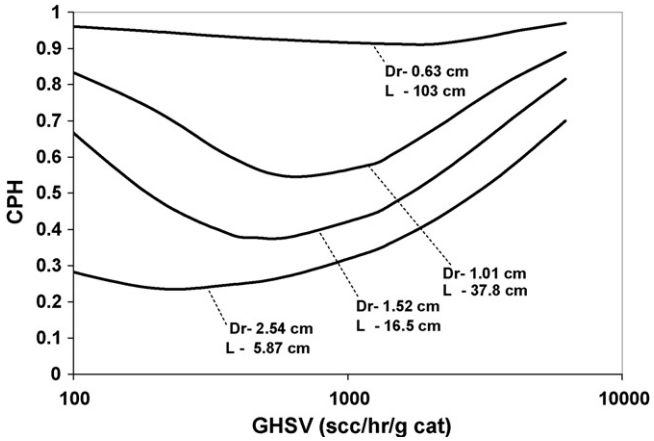

Fig. 16. Model CPH values for various reactor diameters and lengths (fiber diameter kept constant at 2 mm). In each case the amount of catalyst is 29 g (nanopore PBMR at 600 °C, 5 bar total retentate pressure).

Figs. 15 and 16 show the results of another set of extrapolations which were carried out in order to find ways of improving reactor productivity. The reactor diameter was changed similar to the previous exercise, but the membrane fiber diameter was kept constant at 2 mm. The length of the reactor was adjusted such that the amount of catalyst in the reactor remained constant at 29 g. A maximum reactor productivity of ~36 mol/s m^3 was predicted (Fig. 15) for a reactor diameter of 0.63 cm and length of 103 cm. This increase in productivity over the maximum experimental productivity is partly due to the decrease in radial transport time and partly due to the increase in the S_m/V_r ratio which results in a larger membrane surface area. Fig. 16 confirms that the CPH value for the 0.63 cm reactor diameter case is nearly unity for all the space velocities.

Without an optimum reactor design the performance of the membrane reactor may be severely limited by radial diffusion despite using high permeance membrane. Another alternate way of reducing radial transport limitations is the use of multi-fiber reactors. There will be an optimum distance between fibers for which the reactor productivity can be maximized.

6. Conclusions

The decomposition NH_3 was successfully carried out in a packed-bed membrane reactor using both conventional top-layer and nanopore Pd membranes. High-purity H_2 (>99.2%) was obtained from the PBMR. It was determined that H_2 has an inhibitory effect on the rate of NH_3 decomposition on the Ni/Al_2O_3 catalyst used. Due to this kinetic feature, an increase in retentate pressure caused a drop in NH_3 conversion in the conventional packed-bed reactor. However, in the PBMR higher retentate pressures resulted in higher reactor productivities and H_2 utilizations. Moreover, removal of H_2 from the retentate side resulted in an increase in the NH_3 conversion. The experiments revealed that there is an intermediate space velocity for which the reactor productivity is maximum and that at this condition the hydrogen utilization is far from complete. The implication is that one must sacrifice productivity to achieve higher hydrogen utilization, and vice versa. The optimal operating point depends on the trade-off between reactor size and fuel utilization. The former translates to device cost while the latter to energy conversion efficiency.

A two-dimensional model was used to simulate the experimental results, to elucidate the various steps in the H_2 generation and separation processes, and to determine the importance of each step. A comparison of the characteristic times of reaction, flow, radial diffusion and permeation help to identify the limiting steps under different conditions. Overall the rate of radial diffusion limits the productivity of the reactor. Any attempt to increase the productivity has to address this limitation. Just increasing the membrane permeance will not be sufficient in improving the performance of the PBMR. Optimization of reactor dimensions and placement of Pd-membrane fibers in a multi-fiber PBMR are crucial to achieve a high productivity. This is the focus of an ongoing study in our laboratory.

Acknowledgements

We thank the National Science Foundation (CTS-0521977) and the University of Houston for support of this research.

References

[1] S.N. Paglieri, J.D. Way, Sep. Purif. Methods 31 (2002) 1.
[2] G. Saracco, G.F. Versteeg, W.P.M. van-Swaaij, J. Membr. Sci. 95 (1994) 105.
[3] J.R. Lattner, M.P. Harold, Int. J. Hydrogen Energy 29 (2004) 393.
[4] J.R. Lattner, M.P. Harold, Appl. Catal. B: Environ. 56 (2005) 149.
[5] Report of the DOE Workshop on Hydrogen Separations and Purification, September 8–9, 2004.
[6] M.P. Harold, B. Nair, G. Kolios, Chem. Eng. Sci. 58 (2003) 2551.
[7] S.N. Paglieri, I.E. Anderson, R.L. Terpstra, T.J. Venhaus1, Y. Wang, R.E. Buxbaum, K.S. Rothenberger, B.H. Howard, Proc. 20th Annual Conf. Fossil Energy Materials, Knoxville, June 12–14, 2006.
[8] Y. Yildirim, E. Gobina, R. Hughes, J. Membr. Sci. 135 (1997) 107.
[9] S. Uemiya, Top. Catal. 29 (2004) 74–84.
[10] N. Itoh, K. Haraya, Catal. Today 56 (2000) 103.
[11] K.L. Yeung, A. Varma, AIChE J. 41 (1995) 2131.
[12] R.S. Souleimanova, A.S. Muskayan, A. Varma, AIChE J. 48 (2002) 262.
[13] B. Nair, M.P. Harold, J. Membr. Sci. 290 (2007) 182.
[14] S.F. Yin, B.Q. Xu, X.P. Zhou, C.T. Au, Appl. Catal. A: Gen. 277 (2004) 1.
[15] S.T. Oyama, J. Catal. 133 (1992) 358.
[16] T.V. Choudhary, C. Sivadinarayana, D.W. Goodman, Chem. Eng. Sci. 93 (2003) 69.
[17] K. Tamaru, Acc. Chem. Res. 21 (1988) 88.
[18] G. Djega-Mariadassou, C. Shin, G. Bugli, J. Mol. Catal. A: Chem. 141 (1999) 263.
[19] D.G. Loeffler, L.D. Schmidt, J. Catal. 41 (1976) 440.
[20] D.G. Loeffler, L.D. Schmidt, J. Catal. 44 (1976) 241.
[21] A.S. Chellapa, C.M. Fischer, W.J. Thompson, Appl. Catal. A: Gen. 227 (2002) 231.
[22] J. Zhang, H. Xu, W. Li, Appl. Catal. A: Gen. 296 (2005) 257.
[23] T.V. Choudhary, C. Sivadinarayana, D.W. Goodman, Catal. Lett. 72 (3–4) (2001) 197.
[24] J.C. Ganley, E.G. Seebauer, R.I. Masel, J. Power Sources 137 (2004) 53.
[25] T.R. Vencill, A.S. Chellappa, M.R. Powell, Proc. 2nd Int. Fuel cell Science and Engineering Technology Conf., Rochester, NY, USA, June 14–16, (2004), p. 523.
[26] J.P. Collins, J.D. Way, J. Membr. Sci. 96 (1994) 259.
[27] J.P. Collins, J.D. Way, N.A. Kraisuwansaran, J. Membr. Sci. 77 (1993) 265.
[28] E.N. Gobina, J.S. Oklany, R. Hughes, Ind. Eng. Chem. Res. 34 (1995) 3777.
[29] J. Zhang, H. Xu, W. Li, J. Membr. Sci. 277 (2006) 85.
[30] F. Sakaomoto, Y. Kinari, F.L. Chen, Y. Sakamoto, Int. J. Hydrogen Energy 22 (1997) 369.
[31] B.A. Wilhite, M.A. Schmidt, K.F. Jensen, Ind. Eng. Chem. Res. 43 (2004) 7083.
[32] K. Haraya, T. Hatkuta, H. Yoshitome, S. Kimura, Sep. Sci. Technol. 22 (1987) 1425.
[33] S. Hara, K. Sakaki, N. Itoh, Ind. Eng. Chem. Res. 38 (1999) 4913.
[34] B.R.K. Nair, M.P. Harold, J. Membr. Sci 311 (2008) 53.
[35] B.R.K. Nair, J. Choi, M.P. Harold, J. Membr. Sci. 288 (2007) 67.
[36] H.S. Fogler, Elements of Chemical Reaction Engineering, Prentice Hall, Englewood Cliffs, NJ, 1986.
[37] D.J. Gunn, Chem. Eng. Sci. 42 (2) (1987) 363.
[38] R.D. Clayton, M.P. Harold, V. Balakotaiah, Appl. Catal. B: Environ 81 (2008) 161.